Mammal assemblage composition predicts global patterns in emerging infectious disease risk

Wang, Yingying X. G.

2021-10

Wang , Y X G , Matson , K D , Santini , L , Visconti , P , Hilbers , J P , Huijbregts , M A J , Xu , Y , Prins , H H T , Allen , T , Huang , Z Y X & de Boer , W F 2021 , ' Mammal assemblage composition predicts global patterns in emerging infectious disease risk ' , Global Change Biology , vol. 27 , no. 20 , pp. 4995-5007 . https://doi.org/10.1111/gcb.15784

http://hdl.handle.net/10138/334657
https://doi.org/10.1111/gcb.15784

Received: 5 November 2020 | Revised: 13 June 2021 | Accepted: 13 June 2021

DOI: 10.1111/gcb.15784

Global Change Biology WILEY

PRIMARY RESEARCH ARTICLE

Mammal assemblage composition predicts global patterns in emerging infectious disease risk

Yingying X. G. Wang[1,2] | Kevin D. Matson[1] | Luca Santini[3,4,5] | Piero Visconti[6,7] | Jelle P. Hilbers[5] | Mark A. J. Huijbregts[5] | Yanjie Xu[1,8] | Herbert H. T. Prins[1,9] | Toph Allen[10] | Zheng Y. X. Huang[1,11] | Willem F. de Boer[1]

[1]Wildlife Ecology and Conservation Group, Wageningen University and Research, Wageningen, The Netherlands

[2]Department of Biological and Environmental Science, University of Jyväskylä, Jyväskylä, Finland

[3]Department of Biology and Biotechnologies "Charles Darwin", Sapienza University of Rome, Rome, Italy

[4]Institute of Research on Terrestrial Ecosystems (CNR-IRET), National Research Council, Monterotondo (Rome), Italy

[5]Department of Environmental Science, Radboud University, Nijmegen, The Netherlands

[6]International Institute for Applied System Analysis, Laxenburg, Austria

[7]Institute of Zoology, Zoological Society of London, London, UK

[8]The Finnish Museum of Natural History, University of Helsinki, Helsinki, Finland

[9]Department of Animal Sciences, Wageningen University and Research, Wageningen, The Netherlands

[10]EcoHealth Alliance, New York, NY, USA

[11]College of Life Sciences, Nanjing Normal University, Nanjing, China

Correspondence
Willem F. de Boer Wildlife Ecology and Conservation Group, Wageningen University and Research, Droevendaalsesteeg 3a, 6708 PB Wageningen, The Netherlands.
Email: fred.deboer@wur.nl

Zheng Y. X. Huang, College of Life Sciences, Nanjing Normal University, Wenyuan Road 1, Nanjing 210023, China.
Email: zhengyxhuang@gmail.com

Funding information
Chinese Scholarship Council, Grant/Award Number: 201506190134; National Natural Science Foundation of China, Grant/Award Number: 31870400; Jiangsu Higher Education Institutions

Abstract

As a source of emerging infectious diseases, wildlife assemblages (and related spatial patterns) must be quantitatively assessed to help identify high-risk locations. Previous assessments have largely focussed on the distributions of individual species; however, transmission dynamics are expected to depend on assemblage composition. Moreover, disease–diversity relationships have mainly been studied in the context of species loss, but assemblage composition and disease risk (e.g. infection prevalence in wildlife assemblages) can change without extinction. Based on the predicted distributions and abundances of 4466 mammal species, we estimated global patterns of disease risk through the calculation of the community-level basic reproductive ratio R0, an index of invasion potential, persistence, and maximum prevalence of a pathogen in a wildlife assemblage. For density-dependent diseases, we found that, in addition to tropical areas which are commonly viewed as infectious disease hotspots, northern temperate latitudes included high-risk areas. We also forecasted the effects of climate change and habitat loss from 2015 to 2035. Over this period, many local assemblages showed no net loss of species richness, but the assemblage composition (i.e. the mix of species and their abundances) changed considerably. Simultaneously, most areas experienced a decreased risk of density-dependent diseases but an increased

risk of frequency-dependent diseases. We further explored the factors driving these changes in disease risk. Our results suggest that biodiversity and changes therein jointly influence disease risk. Understanding these changes and their drivers and ultimately identifying emerging infectious disease hotspots can help health officials prioritize resource distribution.

KEYWORDS
assemblage composition, climate change, emerging infectious diseases, habitat loss, infectious disease hotspots, species distributions

1 | INTRODUCTION

Emerging infectious diseases (EIDs) threaten public health, animal husbandry, and wildlife conservation (Daszak et al., 2000). The majority of these diseases originate from wildlife (i.e. zoonoses), particularly mammals (Cleaveland et al., 2001). Studying distributions of key wildlife hosts has contributed greatly to our current understanding of EID hotspots (Hay et al., 2013); however, accounting for other co-occurring species within wildlife assemblages is a necessary next step, since the assemblage composition shape transmission dynamics (Chen & Zhou, 2015). Biodiversity is experiencing significant losses globally (McGill et al., 2015), with one quarter of all mammal species threatened by extinction (Díaz et al., 2019). Thus, understanding the links between biodiversity loss and zoonotic disease risk is increasingly urgent.

Many previous studies of diversity–disease relationships have identified host species richness (SR) as a prime driver of disease risk dynamics (Ostfeld & Keesing, 2012). Host SR is linked to reduced disease risk (i.e. the dilution effect) in many different disease systems (Civitello et al., 2015; Huang et al., 2017; Ostfeld & Keesing, 2012). However, the overall direction and strength of the diversity–disease relationship remain unclear (Huang et al., 2016; Wood et al., 2014), with the impact of host SR potentially depending on the type of disease transmission (i.e. density-dependent vs. frequency-dependent; Dobson, 2004; Joseph et al., 2013). In addition to SR, the composition of local species assemblages (i.e. which species are present and at what abundances) can also influence disease risk (Chen & Zhou, 2015) as species vary considerably in their host competence (i.e. their ability to transmit a pathogen to another susceptible host; Merrill & Johnson, 2020). For example, wildlife communities with more abundant high-competence hosts would show higher disease risk compared with communities with more abundant low-competence hosts. However, rare studies integrated host abundance in mapping zoonotic disease risk (Keesing & Ostfeld, 2021).

Variation in host competence may relate to variation in life history and its proxies, such as body mass (Merrill & Johnson, 2020). For instance, small-bodied species tend to have a higher host competence than larger-bodied ones (Huang et al., 2013; Johnson et al., 2012). Moreover, larger species of mammals generally have higher neutrophil concentrations, indicating stronger immune defences (Downs et al., 2020). This relationship between body mass and competence could arise via two mechanisms (Joseph et al., 2013). First, life-history theory suggests that short-lived (usually relatively small) species invest more in reproduction and less in immune defences (Cronin et al., 2014). Smaller species may therefore be more susceptible to infection (Ricklefs & Wikelski, 2002). Second, the parasite local-adaptation theory suggests that parasites evolve to exploit the most common species, which are also usually relatively small. This evolutionary response is driven by selective pressures associated with the loss of host species during community disassembly (Ostfeld et al., 2014). Negative relationships between body mass and host competence have been reported in multiple pathogen systems, including *Borrelia burgdorferi* (Banerjee et al., 2017; Ostfeld et al., 2014), Eastern equine virus (Huang et al., 2013), West Nile virus (Banerjee et al., 2017; Huang et al., 2013), and *Ribeiroia ondatrae* (Johnson et al., 2012). Recently, the negative relationship between body mass and host competence has also been detected across orders (Downs et al., 2020). While other factors (e.g. sociality and gregariousness (Altizer et al., 2003) may also influence host competence, body mass is the most commonly used proxy.

Life history and its proxies predict not only host competence but also the population sizes of species. Larger species are rarer than smaller species due to the high energetic requirements associated with large body mass (Damuth, 1981; Silva & Downing, 1995). Likewise, carnivores tend to be rarer than similarly sized herbivores due to lower resource availability and energy conversion efficiencies (Silva et al., 1997). The size of suitable habitat also influences animal population sizes, and its loss typically translates into population declines. Population declines (and related increases in relative abundances of other members of the assemblage) typically occur well before local extinctions (Gaston & Fuller, 2008; Hillebrand et al., 2008). Shifts in assemblage composition can therefore affect disease risk before changes in SR. Understanding these effects can provide insights into spatial patterns in disease risk among wild animals, thereby facilitating predictions about EID outbreaks (Jones et al., 2008).

We conducted a three-pronged analysis (Figure S1) to study global patterns both in disease risk and in biodiversity-associated changes this risk. First, we mapped a global disease risk based on species distribution and abundance projections of

4466 mammal species, and we identified current hotspots of disease risk (per grid cell, 0.5° resolution, 55 km at the equator). We then compared this map (i.e. per grid cell) with the risk pattern of EID events originating from wild mammal species (Allen et al., 2017). Second, we forecasted future hotspots of disease risk using mammal assemblages predicted for the year 2035 under two different shared socioeconomic pathways (SSPs; O'Neill et al., 2014). These SSPs integrated a combination of climate model projections, socioeconomic conditions, and possible climate policies. The first scenario (SSP1) assumes low human population growth, proactive environmental protection, and low vulnerability to climate change; the second scenario (SSP3) assumes the opposite (high population growth, reactive environmental protection, and vulnerabilities to climate change that vary regionally). Third, we analysed the impact of assemblage composition variables (e.g. SR and evenness in abundance), changes in these variables, and their interactions on disease risk (i.e. community R0).

2 | MATERIALS AND METHODS

We first modelled species distribution of 4466 mammal species in the year of 2015 and projected it for the year of 2035 with a resolution of 0.5° at global level (Figure S1). For each time step, we predicted the average population density of each species to estimate mammal assemblage composition in each cell. For species distribution (Section 2.1), we obtained species geographical range from IUCN and derived climate data from the Intergovernmental Panel on Climate Change (IPCC) Fifth Assessment Report (AR5) project (Section 2.1.1). We applied bioclimatic envelope models to investigate the relationships between climate and species geographical ranges, and then predicted species distributions for the years of 2015 and 2035 (Section 2.1.2). We estimated the Area of Habitat (AOH) within the predicted distribution using habitat preferences rules (Section 2.1.3). We then predicted the average species abundance within species' habitats using population density models with taxonomic information and species traits (body mass and diet) as predictors, and constructed the mammal assemblage for each grid cell for the years 2015 and 2035 (Section 2.2). For each mammal assemblage, we then applied a multi-species SIR model to calculate the community-level basic reproductive ratio, community R0, as a measurement of disease risk (Section 2.3). Community R0, which is positively related to maximum infection prevalence, can be used as a proxy for pathogen invasion and persistence (Dobson, 2004). Community R0 has been widely used in previous theoretical studies on diversity–disease relationships (Chen & Zhou, 2015; Joseph et al., 2013). We compared this current disease risk map with the risk pattern of EIDs originating from wild mammals (Allen et al., 2017) to estimate its predictive accuracy (Section 2.4). Finally, we used General Linear Models (GLMs) to explore the factors driving the changes in disease risk between the current and future (Section 2.5).

2.1 | Species distribution

2.1.1 | Climatic variables

To simulate climate change effects on the distribution of mammal species, we first derived climatic conditions from the IPCC AR5. We used three future scenarios Representative Concentration Pathway (RCP) simulations (3, 4.5, and 8.5 W/m^2 of radiative forcing), respectively compatible with 0.4–1.6, 0.9–2.0, 1.4–2.6 average degree warming with respect to the 1986–2005 average. The three RCPs considered were combined with two shared SSPs. The first, SSP1, assumes low challenges for mitigation and adaptation (i.e. low human population growth, proactive environmental protection, and low vulnerability to climate change). The second, SSP3, assumes high challenges for mitigation and adaptation (i.e. high population growth, reactive environmental protection, and vulnerabilities to climate change vary regionally). For each scenario, we used 17 General Circulation Models (GCMs; Table S6) in climate change projections, and then calculated the median value of 14 bioclimatic variables (Table S5) across 17 GCMs to account for the large uncertainties between different models (Rowlands et al., 2012). Projecting species responses for each of the individual GCMs is computationally impractical and time-consuming; however, the observed trends are very closely tracked the ensemble median (Ameca y Juárez et al., 2013). The median bioclimatic variable layers were derived for two time points: 2015 and 2035. For consistency with the standard procedure used to prepare present bioclimatic variables and to reduce the influence of outliers, each year was calculated as an average over a 30-year period, that is, 2000–2030 for 2015, and 2020–2050 for 2035.

2.1.2 | Bioclimatic envelop modelling

We estimated the effects of climatic variables on species distribution by fitting bioclimatic envelopes at 0.5° resolution for 3,031 terrestrial mammal species. For another 2033 species, we assumed constant ranges over time. We made this assumption because their current range was either too small to sample at least 30 presence points for fitting bioclimatic envelope models or their ranges almost entirely occupied an entire landmass, and therefore we could not draw sufficient pseudo-absence points to fit these models. Furthermore, 598 species were excluded from the analysis, as there were no range maps available so that the species could not be modelled. We used two statistical models, Generalized Linear Models and Generalized Additive Models (Beaumont et al., 2016), to fit current bioclimatic envelopes and project these envelopes for both SSP1 and SSP3. We allowed the algorithm to fit up to a third-order polynomial of each variable in the GLM and fit cubic splines at each knot in the GAM.

We obtained the presence points to fit the models by systematically sampling one point location at each grid cell within the current species current range (IUCN, 2015). This method of modelling

bioclimatic envelopes allows robust projections of species responses to climate changes (Hof et al., 2018; Newbold, 2018; Thuiller et al., 2019; Visconti et al., 2016). To avoid creating pseudo-absences in areas of potentially suitable climate falling outside the reach of the species, pseudo-absence points were obtained by systematically sampling areas outside the current species' current range but within the same continents/islands and the same biogeographical region (prediction extent). We drew a random sample of pseudo-absences equal to the minimum between 80% of unoccupied grid-cells within the prediction extent, and 1000 pseudo-absences. For each model, presences and absences were weighted in order to reach a prevalence of 0.5 in the training dataset. This pseudo-absence draw was performed five times. For each draw, we repeated three times a bootstrapping procedure by keeping 80% of the data to calibrate the model and using the remaining 20% for validation (Newbold, 2018). Therefore, we had 30 models in total for each species, year and climatic scenario from the combination of two statistical models (GLM and GAM), five pseudo-absences draws, and three input data resamples. We binarized the probabilistic models using the probability thresholds that maximized the True Skill Statistic (TSS; Allouche et al., 2006), which is equal to sensitivity (true presence rate) plus specificity (true absences rate) minus 1. TSS varies from −1 to 1 with 0 meaning a predictive capacity close to random and values >0.5 and >0.8 are generally recognized as indicating good and very good predictive capacity, respectively. For each species, year, and climatic scenario, we combined all bioclimatic envelope models with a TSS>0.8 (obtained from the bootstrapping procedure) by taking the ensemble mode value (between predicted presence and absence) for each grid cell so that the final mode value was the consensus of only high-performing models.

2.1.3 | Quantifying the AOH

Species distributions were estimated based on suitable climate conditions using Bioclimatic envelope models (Section 2.1.2). However, within this distribution, the habitat may not be suitable. IUCN habitat preference rules were then applied to identify and quantify the AOH for each species within the species' distribution (Brooks et al., 2019; Rondinini et al., 2011; Santini et al., 2019; Visconti et al., 2011, 2016). The variables considered in the models were the elevation, land cover, and land-use type. Each combination of land cover and land-use was scored as either suitable or not according to IUCN expert knowledge (Rondinini et al., 2011), based on the habitat preference and the tolerance to human disturbance collected from IUCN Red List data. This exercise reflects what is known in the literature about the species according to experts; some level of subjectivity can be present. Another limitation is the inconsistency in the level of knowledge across a wide range of species. Despite the fact that results might be influenced by the available knowledge on the species, this approach is commonly used to quantify the species' AOH of many species globally (Jung et al., 2020). It allows to use species-specific information and reduces the over-estimation of available habitat area due to the consideration of climate only in climatic envelope models (Visconti et al., 2016).

Following this approach, only climatically suitable grid cells with suitable habitat were considered for abundance predictions (Section 2.2). In total, we had 4466 species of terrestrial mammals for which range data and habitat preferences were available to produce habitat suitability models. For the 3031 species for which bioclimatic envelopes were possible, we took the conservative assumption that species were not able to colonize newly suitable habitat that was not in the list of current suitable habitat types for each of the species.

2.2 | Population abundance predictions

To predict species population abundance within suitable habitat, we constructed predictive models based on the density records from the TetraDENSITY database (Santini et al., 2018a) following (Santini, Isaac, Maiorano, et al., 2018). The density records we collected included 12,209 records of 717 mammalian species. These density records were estimated using different methods (e.g. mark–recapture, distance sampling, census, etc.). For each species and sampling method, we obtained the median population density, resulting in a dataset of 1171 estimates. The predictive models were obtained by fitting mixed-effects models with body mass and diet information from the EltonTrait database (Wilman et al., 2014) as fixed predictors. For diet variables, we considered the percentage of seven diet items for all species: carnivory (sum of fish, ectotherms, endotherms, and unknown categories), insectivory, scavenging, nectarivory, frugivory, granivory, and consumption of other plant items (herbivory/folivory). Population density and body mass variables were log10-transformed prior fitting models. We considered a cubic term for body mass (Silva & Downing, 1995) and a quadratic term for all diet variables. We included taxonomic order, family, and species as nested random effects to account for taxonomic relatedness and average differences in population density in different taxonomic groups (Santini, Isaac, Maiorano, et al., 2018). We also included an additional random effect for the sampling method, encompassing broad categories of methods for estimating population density (Santini, Isaac, Maiorano, et al., 2018). We ran a full model selection based on predictive accuracy of models (Santini, Isaac, Maiorano, et al., 2018): we validated each model using a taxonomic-block validation at the level of taxonomic orders (Roberts et al., 2017), iteratively fitting the model on all but one taxonomic order and validating the model the order excluded. This allowed us to quantify the predictive error when extrapolating on species outside the sample in terms of minimum absolute error (MAE). We selected the models with the lowest average MAE per taxonomic order weighted by the number of species per order. The model with the highest predictive accuracy was:

$$\begin{aligned}\text{Density} \sim \text{BM} + I(\text{BM}^2) + I(\text{BM}^3) + \text{Inv} + \text{Carn} \\ + (1|\text{Order/Family/sp\_id}) + (1|\text{Method}),\end{aligned} \quad (1)$$

TABLE 1 The definitions and values of parameters used in SIR model

Parameter	Definition	Value
w_i	Body mass of species *i*	Obtained from EltonTrait database (Wilman et al., 2014)
b_i	Birth rate of species *i*	$0.4w_i^{-0.26}$
d_i	Death rate of species *i*	$0.4w_i^{-0.26}$
N_i	Abundance of species *i*	From the species abundance projections
v_i	Disease-induced mortality	$0.5d_i$
R_{0i}	Intraspecific basic reproductive rate	$\sim \Gamma(k, \theta)$
k	Shape parameter for Gamma distribution	0.5
θ	Scale parameter for Gamma distribution	1.5
β_{ii}	Intraspecific transmission rate	$R_{0i} \times (d_i + v_i + r_i)/N_i$
β_{ij}	Interspecific transmission rate	$c \times (\beta_{ij} + \beta_{ji})/2$
c	Interspecific transmission scaling coefficient	0.05
r_i	Recovery rate	10

Abbreviation: SIR, susceptible–infected–recovered.

where density = log10 (population density), BM = log10 (body mass), Inv = Percentage of invertebrates in diet, and Carn = Percentage of carnivory in diet (Table S7).

Using this model, we predicted the average population density for all mammal species. In addition to the fixed effect component of the model (body mass and diet), the predictions were also informed by the random effects that modelled consistent deviations from the intercept for taxonomic orders, families, and species hierarchically, therefore accounting for latent variables. When a taxonomic level for a species was not present in the models, the respective random effect was set to zero. We then multiplied the population density values by the predicted AOH of the species within each grid cell to obtain an estimate of population size. These average estimates of population are not aimed to provide the real population size of species at each location, as they can be influenced by many local conditions (e.g. biotic interactions, demographic fluctuations, human disturbances, etc.), but rather provide a coarse estimate of assemblage structure based on species average abundances. With the predicted species distribution and abundance in the years 2015 and 2035, we then calculated, for each grid cell, the number of species gained (i.e. new species occurring), the number of species lost (i.e. locally extinct), the number of species remaining, and the change (%) in animal abundance per species group between 2015 and 2035 (Tables S3 and S4). Changes in mean animal abundance of species were measured as abundance in 2035 minus abundance in 2015 divided by the abundance in 2015.

2.3 | Calculation of disease risk (community R0)

2.3.1 | SIR model

We constructed a multi-species SIR (susceptible–infected–recovered) model (Dobson, 2004) to simulate pathogen transmission of each assemblage in 2015 and 2035:

$$\frac{dS_i}{dt} = b_i N_i - d_i S_i - p_i \sum_{j=1,\ldots,n} \beta_{ij} I_j,$$

$$\frac{dI_i}{dt} = p_i \sum_{j=1,n} \beta_{ij} I_j - (d_i + v_i + r_i) I_i,$$

$$\frac{dR_i}{dt} = r_i I_i - d_i R_i,$$

where the population size of species, *i* (N_i), was divided into three compartments, that is, susceptible (S_i), infected (I_i), or recovered (R_i), could be obtained from our abundance projections. We assumed assemblages at equilibrium, which means each species had identical birth rate (b_i) and death rate (d_i). We assumed no vertical transmission and infection could cause an additional mortality (v_i). Infected hosts could be recovered and immune at a recovery rate r_i. The intraspecific transmission rate β_{ii} was derived from the intraspecific reproductive number R_{0i} (Section 2.3.2), which could be considered as a measure of host competence (Chen & Zhou, 2015; Joseph et al., 2013). Following previous studies (Chen & Zhou, 2015; Dobson, 2004; Joseph et al., 2013; Rudolf & Antonovics, 2005), we assumed symmetrical interspecific transmission rates $\beta_{ij} = \beta_{ji} = c\ (\beta_{ii} + \beta_{jj})/2$, where parameter *c* is a scaling factor regulating the strength of interspecific transmission. The definitions for parameters are listed in Table 1.

2.3.2 | Parameters in SIR model

Studies have suggested that the population size, birth rates, and death rates of most vertebrate species tend to scale allometrically with their body mass (Peters, 1986). A previous study scaled the epidemiological parameter values as functions of host body size in a variety of epidemiological models, and demonstrated that these

allometric relationships provide useful estimates for transmission rate (β_{ii}) of mammals over a wide range of body mass (De Leo & Dobson, 1996). We, therefore, assumed that both the epidemiological and demographic parameters follow allometric relationships. For each mammal species, body mass estimates were obtained from the EltonTrait database (Wilman et al., 2014).

As many studies showed that host competence was negatively correlated with body mass, we here, following previous studies (Chen & Zhou, 2015; Joseph et al., 2013), draw the intraspecific reproductive ratio R_{0i} from a right-skewed truncated gamma distribution with a scale parameter $\theta = 1.5$ and a shape parameter $k = 0.5$. In this distribution, only a small fraction of R_{0i} values were larger than 1, meaning that only a few host species could sustain infectious diseases. The pattern of R_{0i} generated by this assumption was consistent with observations from many plants and wild animal populations (Joseph et al., 2013). Values of R_{0i} were then sorted and assigned to each species by assuming reverse-rank ordering between body mass and intraspecific R_{0i} (Chen & Zhou, 2015; Joseph et al., 2013) so that smaller species were better competent hosts than larger ones. The values for other parameters were drawn from previous studies (Chen & Zhou, 2015; Joseph et al., 2013) and listed in Table 1.

2.3.3 | Community R_0

Based on the constructed SIR model, we calculated, for each local mammal assemblage (i.e. the species assemblage in a 0.5° grid cell), the community R0 to measure disease risk. The community R0 could be calculated as the dominant eigenvalue of the next-generation matrix (G):

$$G = \begin{bmatrix} \frac{\beta_{ii}p_i}{(d_i+v_i+r_i)} & \cdots & \frac{\beta_{ij}p_i}{(d_i+v_i+r_i)} \\ \vdots & \ddots & \vdots \\ \frac{\beta_{ji}p_j}{(d_j+v_i+r_j)} & \cdots & \frac{\beta_{jj}p_j}{(d_j+v_i+r_j)} \end{bmatrix}.$$

Community R0 is generally positively related to the maximum infection prevalence in the assemblage and has been widely used in theoretical studies to estimate the probability of pathogen invasion and persistence (Joseph et al., 2013). Parameter p_i determines whether the transmission is density-dependent or frequency-dependent. For density-dependent diseases, the p_i term corresponds to the abundances of the susceptible host species i (S_i); while for frequency-dependent diseases, the p_i term corresponds to the relative abundances of susceptible host species i (S_i/N).

2.4 | Comparison of the prediction

To estimate the accuracy of our analyses, we compared our predicted community R0 values from 2015 with zoonotic EID risk calculated from observed outbreaks in wildlife from 1970 to 2016. The zoonotic EID risk (Allen et al., 2017) is the probability of a grid cell having an EID event after correcting for differences in variables related to reporting effort and human population (Allen et al., 2017). The latter step was necessary because spatial patterns of reported EIDs can be biased by incomplete spatial distribution of detection and reporting efforts (e.g. related to differences in gross domestic product). We constructed a General Linear Mixed Model with EID risk as the dependent variable and community R0 from both density-dependent and frequency-dependent diseases as predictors. We included continent as the random factor by assuming that disease risk patterns differ among continents.

2.5 | Statistical analyses

We used GLMs to explore the factors responsible for changes in community R0 (ΔR0) under different scenarios (i.e. SSP1 and SSP3; Table S2) for diseases with both density-dependent and frequency-dependent transmission. For predictors, we included original SR, which is the number of different species within local assemblage in 2015; original species evenness (EV), which is Pielou's evenness index (J') calculated as the Shannon index divided by the maximum of Shannon index.

We also considered the original percentage of large species (PL), measured as the percentage of abundance of species with body mass larger than 3 kg (Cardillo et al., 2005). The extinction risk in large mammals and small mammals are generally driven by different factors (Cardillo et al., 2005; González-Suárez et al., 2013). Species with body mass <3 kg are mainly threatened by external threats, for example, size of geographical range and human population density, while larger species are more vulnerable to extinction because of the combination of external threats and intrinsic traits (Cardillo et al., 2005). We also included the change in each of these variables: ΔSR, ΔEV, ΔPL, between 2015 and 2035. We quantified changes in assemblage composition over time, such as changes in SR (ΔSR) as $\Delta SR = \ln(SR_{2035}/SR_{2015})$. Changes in R0 over time were calculated similarly: $\Delta R = \ln(R0_{2035}/R0_{2015})$. To compare the effect sizes of different predictors, we standardized all explanatory variables (mean = 0 and SD = 1). In these GLMs, we included diversity indices, changes in both types of indices over time, and all two-way interactions between a given index and its change.

3 | RESULTS

3.1 | Global distribution of community R0

Our results indicate that disease risk, as indexed by community R0, varies geographically at global scale. Risk of density-dependent diseases was high in tropical and north temperate regions (Figure 1a); in contrast, risk of frequency-dependent diseases was high in the northernmost parts of North America and Eurasia and in Oceania (Figure 1b).

Overall, our mixed model (with continent as a random factor) explained 68% of the variation (conditional R^2) in global EID risk, which

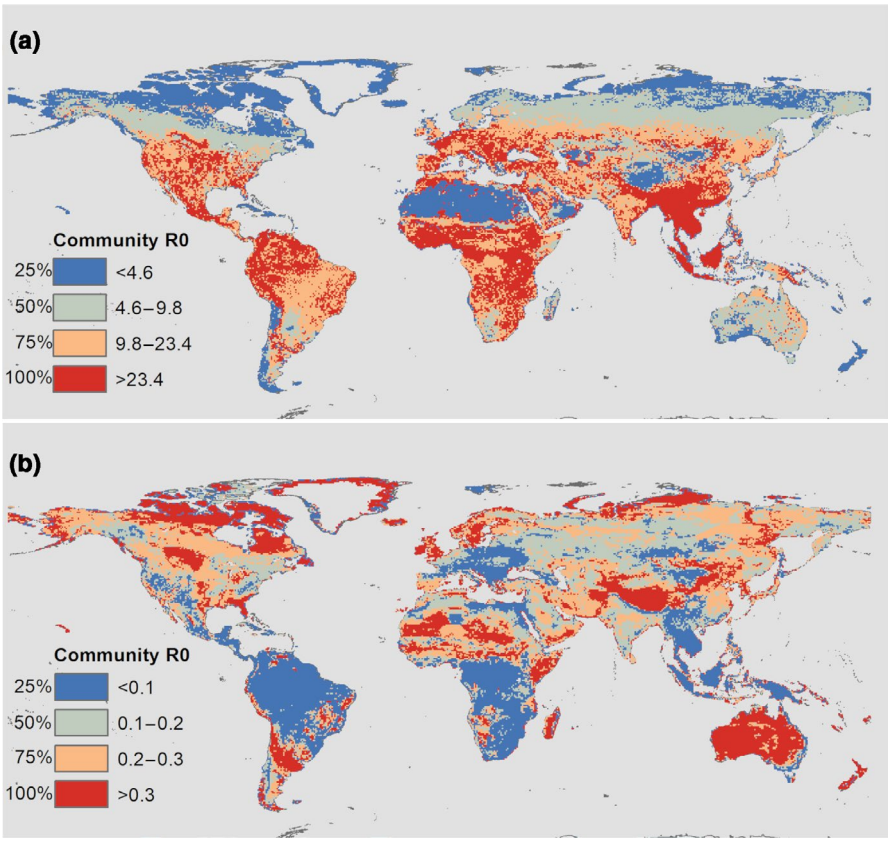

FIGURE 1 Spatial differences in the predicted community R0 with quantiles for (a) density-dependent and (b) frequency-dependent diseases in 2015. Red signals high disease risk; blue signals low disease risk

was estimated from a global database of EID events. Community R0 explained 29% of the variation (marginal R^2) in density- and frequency-dependent diseases (Figure 2; Figure S2; Table S2). Predictive accuracy of our model varied among continents. For example, fixed factors explained 47% variation for North America, but only 0.06% for Asia. In Oceania, community R0 of frequency-dependent diseases explained (14%) better than density-dependent ones (5%).

3.2 | Future changes in mammal assemblages and community R0

To forecast future changes in disease risk, we calculated how mammal assemblage composition changed from the year of 2015 and 2035 under more severe (SSP3) and less severe (SSP1) climate change scenarios. As expected, the SR of local assemblages decreased more under SSP3 (Figure 3a,c). Furthermore, while many local assemblages did not show net losses of richness under either scenario because colonizations counteracted extinctions (Tables S3 and S4), assemblage composition (i.e. the mix of species and their abundances) changed considerably (Figure 3b,d).

Rodent species dominated most assemblages (Tables S3 and S4). On average, 30 rodent species per grid cell remained in 2035 under both scenarios, but the mix of species changed. Compared to other orders, more rodent species were lost (i.e. went locally extinct; mean number of species per grid cell SSP1: 3.20; SSP3: 3.50), and more were gained (i.e. via colonization; mean number of species per grid cell SSP1: 0.98; SSP3: 0.04). Orders with relatively small-bodied species showed larger increases in mean abundance (e.g. 92% increase for the Australian Peramelemorphia, 60% increases for Lagomorpha) compared to orders with relatively large-bodied species (e.g. 0% increase for Macroscelidea) under SSP1 (Table S3). The majority of orders decreased in terms of mean abundance under SSP3. Rodentia increased by 12% (Table S4).

The disease risk of local assemblages (i.e. community R0) changed between 2015 and 2035 in ways that depended on disease transmission type (Figure 4). The risk of density-dependent diseases decreased in most areas under both SSP1 and SSP3 (Figure 4a,c). Exceptions (thus, increased community R0) under SSP1 included parts of Europe, eastern South America, the central part of Africa, and eastern Asia; exceptions under SSP3 included scattered areas in Southern America and the central part of Africa. The risk of frequency-dependent diseases increased in most areas under both SSP1 and SSP3 (Figure 4b,d). Only a few areas in north and central Africa showed a decrease in community R0.

3.3 | Factors driving the changes in disease risk

We explored the factors driving the changes in risk of both density-dependent and frequency-dependent diseases (Figure S3). Generally, *changes* in assemblage composition (i.e. differences in SR and evenness between 2015 and 2035) had larger effects than the original 2015 values of those indices. The risks of both density- (Figure 5b) and frequency-dependent diseases (Figure 5e) were significantly related to the interaction between original species evenness in 2015

and the change in species evenness between 2015 and 2035 (i.e. EV*ΔEV). When original evenness was high, further increases in evenness led to strong declines in disease risk for both transmission types.

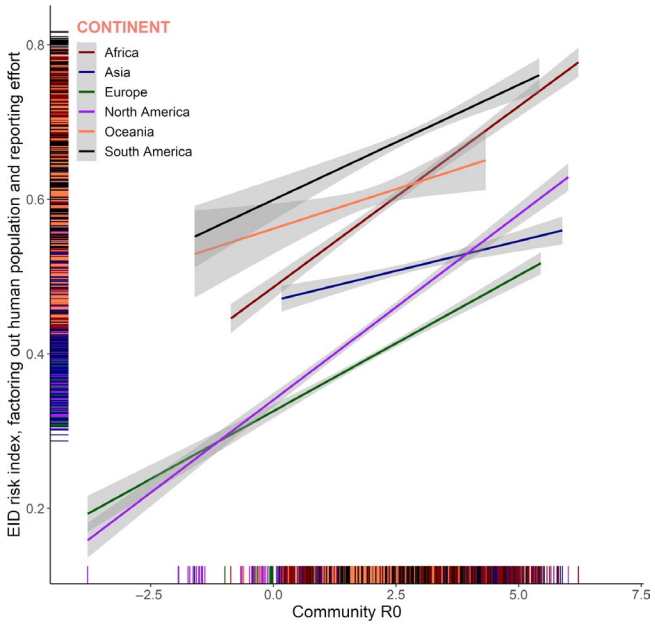

FIGURE 2 Relationships (regression ± 95% CIs) between predicted community R0 for density-dependent diseases and reported Emerging infectious disease (EID) risk index per grid cell from General Linear Mixed Models. Marginal rugs indicate the density of EID risk index and community R0

The risks of both density- and frequency-dependent diseases were also significantly related to the interaction between original SR and the change in SR (i.e. SR*ΔSR). However, the effect differed considerably between the two transmission types. With density dependence, when original SR was relatively low, a decline in SR led to a decrease in disease risk (Figure 5a). With frequency dependence, a decline in SR led to an increase in disease risk when original SR was relatively low; however, when the original SR was high, a decline in SR led to nonlinear changes in disease risk (i.e. first an increase, then a decrease; Figure 5d).

4 | DISCUSSION

4.1 | Hotspots and changes of disease risk

We estimated spatial patterns of disease risk for both density- and frequency-dependent diseases from mammal assemblages. Those spatial patterns were quantitatively consistent with the patterns of EIDs originating from wild mammals (Allen et al., 2017). In addition to previously identified high-risk areas in the equatorial tropics (Allen et al., 2017; Hay et al., 2013), we also identified high-risk areas in temperate Europe, North America, and Asia for density-dependent diseases and in the northernmost parts of North America and Eurasia and in Oceania for frequency-dependent diseases. In the case of density-dependent diseases, the identified temperate areas align with other previous work that suggests that areas in northern latitudes have

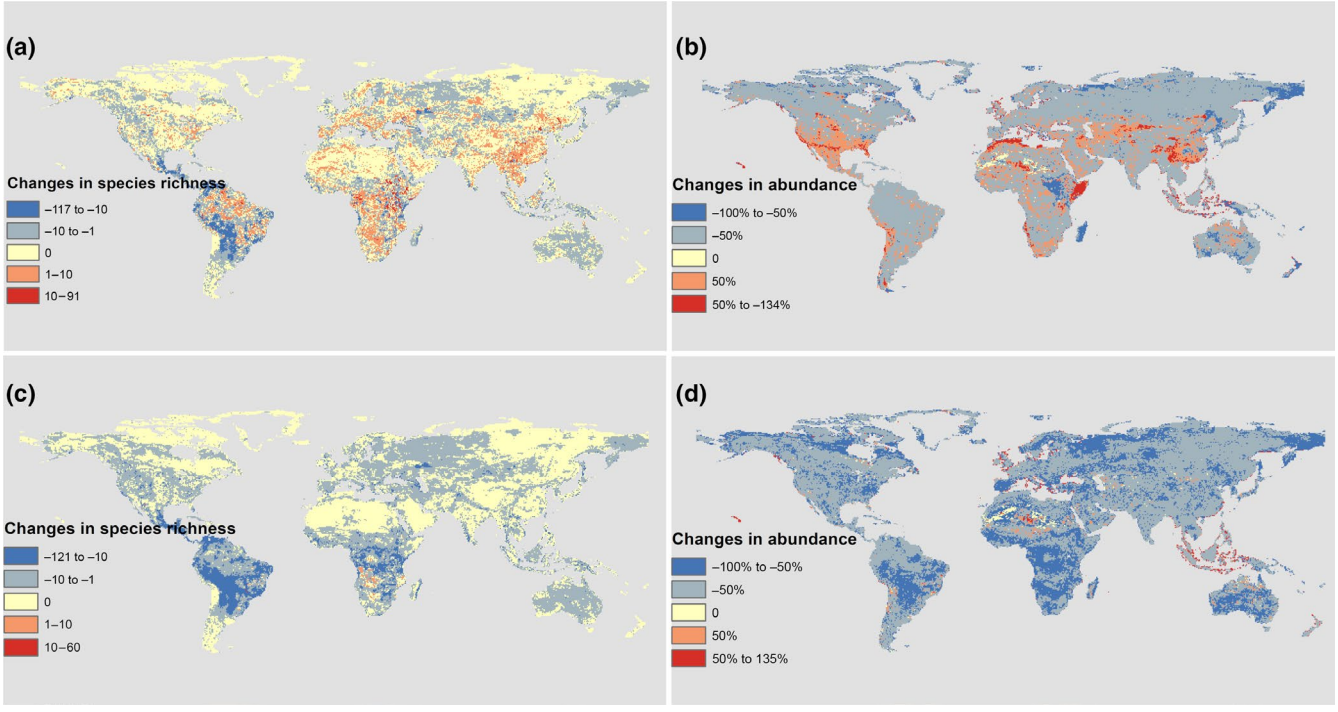

FIGURE 3 Changes in species richness (SR; a, c) and changes in mean animal abundance (%; b, d) for 2 years (2015 and 2035) under climate change scenario SSP1 (a, b) and SSP3 (c, d). Changes in SR were measured by comparing SR simulated for 2015 and 2035. Changes in mean abundance were measured by comparing geometric mean abundance simulated for 2015 and 2035. Red and orange indicate increased richness or abundance; blue and grey indicate decreased richness or abundance; yellow indicates constant richness or abundance

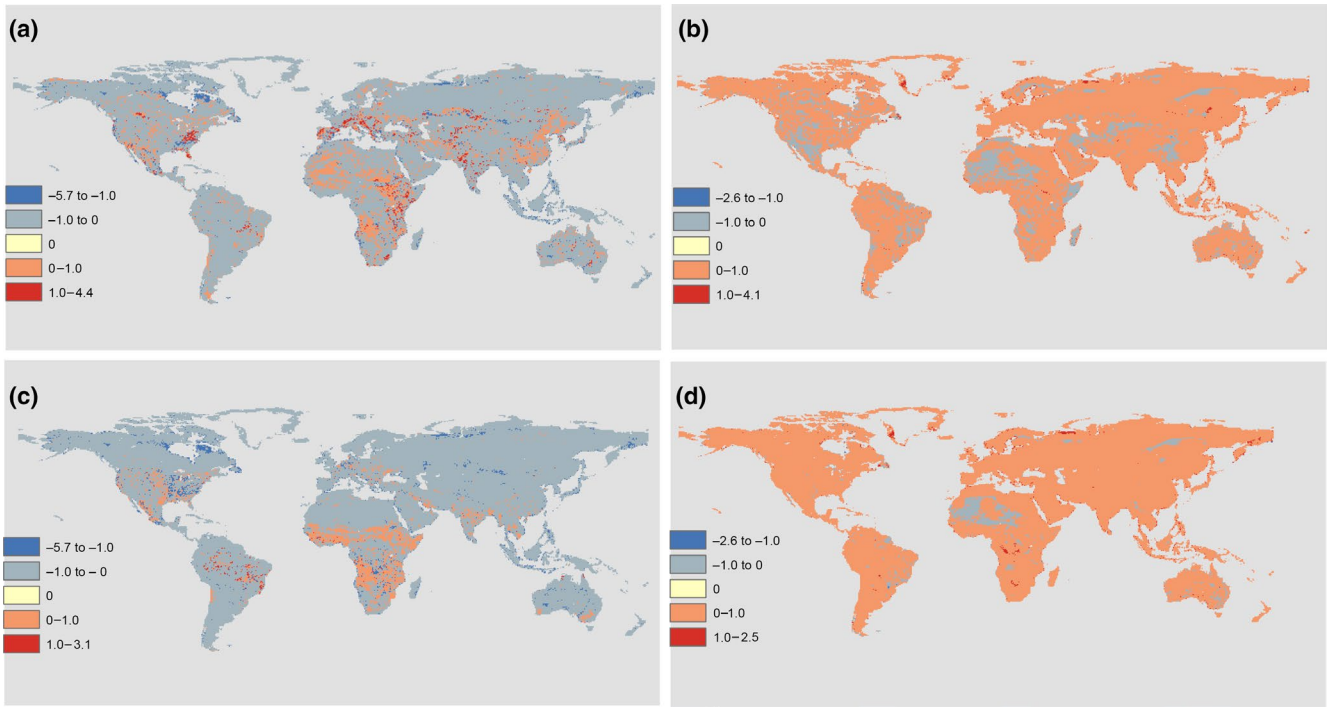

FIGURE 4 Changes in community R0 ($\ln(R0_{2035}/R0_{2015})$) for density-dependent (a, c) and frequency-dependent (b, d) diseases under scenario SSP1 (a, b) and SSP3 (c, d) from 2015 to 2035

more zoonoses (Han et al., 2016), potentially because mammal species assemblages in temperate Europe, North America, and Asia areas have relatively higher rates of viral sharing (Albery et al., 2020). In the case of frequency-dependent diseases, the areas we identified align well with observed distributions of tick-borne diseases in humans (www.gideononline.com). For example, Anaplasmosis and Lyme disease are mainly reported in United States of America, Canada, Russia, and Australia. Also found specifically in Australia are Flinders Island spotted fever and Queensland tick typhus.

One possible explanation for this disease risk pattern is that high-risk areas are characterized by higher abundance or relative abundance of small-bodied species (i.e. competent hosts, such as Rodentia, Figures S4a and S5a; Gibb et al., 2020), and lower relative abundance of large-bodied species (i.e. incompetent hosts, such as Cetartiodactyla, Figure S5c). Our approach to predicting disease risk sheds new light on possible mechanisms underlying EID risk. Since these smaller species are more competent than other larger species for generalist pathogens (Huang et al., 2013; Johnson et al., 2012), assemblages containing more of these species have higher values of community competence. Also, mammal species in northern latitudes have been suggested to carry more zoonoses and share more viruses compared to species in other regions (Albery et al., 2020; Han et al., 2016). As the existence of large species may regulate both the absolute and relative abundance of smaller species due to interspecific interactions (e.g. competition and predation), we consider that conserving larger species could serve as an important control measures infectious diseases.

Disease risk changed under the influence of the biodiversity changes predicted by SSP1 and SSP3. Changes in the risk of density-dependent diseases were related to changes in the abundance of relatively small species (e.g. Rodentia and Chiroptera), which globally increased abundance under SSP1 but often decreased under SSP3 (Figures S6a,b and S7a,b). More areas showed an increased risk of frequency-dependent diseases under SSP3 and SSP1 because these frequency-dependent diseases are more sensitive to the changes in the relative abundance of large species. Larger species with slower growth rates are more likely to go locally extinct when conditions are unsuitable (Tomiya, 2013; e.g. under SSP3; Figures S9c,d).

4.2 | Drivers for the disease risk changes

The impact of biodiversity loss on disease risk is a subject of debate (Halliday & Rohr, 2019; Halliday et al., 2020; Huang et al., 2016; Liu et al., 2020; Randolph & Dobson, 2012; Rohr et al., 2020; Salkeld et al., 2013; Wood & Lafferty, 2013; Wood et al., 2014). Some studies suggest that high biodiversity protects people from infectious diseases and that species loss increases disease risk (Civitello et al., 2015; Huang et al., 2017); other studies suggest biodiversity would be more likely to increase disease risk (Wood et al., 2014). We studied the effect of biodiversity changes, both gains and losses, on disease risk. Disease risk was related to the interaction between the original SR and the change in SR. Our result suggested that the dilution effect might be more common in species-poor assemblages: with relatively low original SR, further loss of species increased diseases risk. This result lends support to existing ideas that highly competent species dominate low diversity systems that have suffered species losses (Johnson et al., 2019).

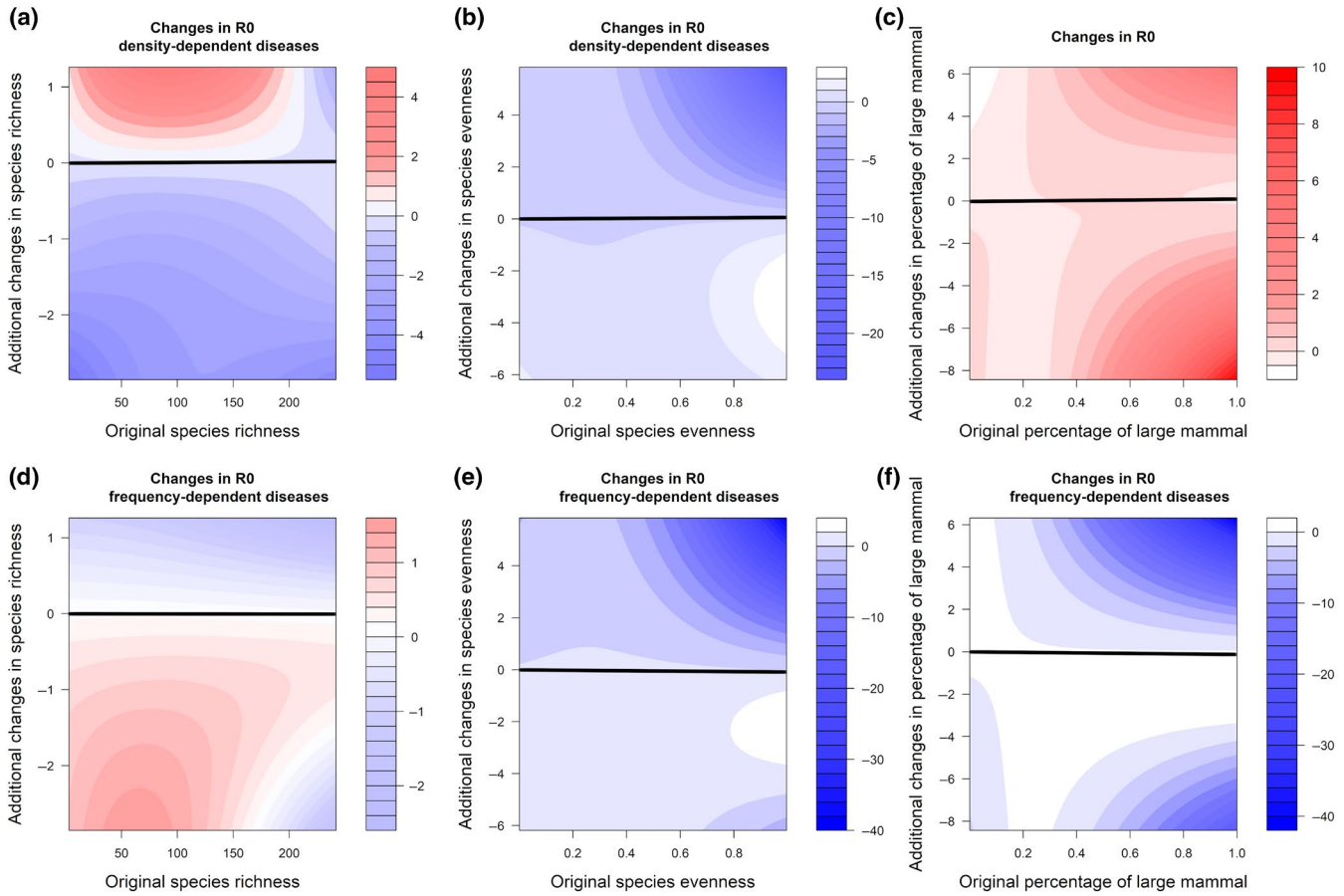

FIGURE 5 Surface maps showing interaction effects between original values of a predictor (*x*-axis) and changes of that predictor (*y*-axis) on changes of community R0 for density-dependent diseases (a–c) and the frequency-dependent disease (d–f). Values on the y-axis above zero (black line) indicate increase in predictors, and values below zero indicate decrease in predictors. Colour and colour intensity indicate changes in R0: blue indicates decreased disease risk; red indicates increased disease risk

The effect of original evenness and change in evenness is more important than the effect of SR. Decreasing evenness generally increased disease risk for both frequency-dependent and density-dependent transmitted diseases, which is consistent with a previous study (Chen & Zhou, 2015). Assemblages with decreased evenness might be dominated by several abundant species, for example from Rodentia, which generally have higher intraspecific contact rates and viral-sharing rates (Albery et al., 2020). Ultimately, intraspecific and interspecific transmission of pathogens (and thus disease risk) would be higher in those more uneven assemblages.

5 | CONCLUSIONS

We estimated global disease risk based on the compositions of mammal assemblages, which were generated using species distribution modelling and predicted average abundance distributions. We modelled species abundances using well-known allometric relationships, which do a good job of approximating global geographical patterns. Nevertheless, certain nuances in species abundances, for example, due to habitat quality, species interactions, and biological factors beyond body mass and diet, were undoubtedly missed. These factors and others, including dispersal and demography, can also influence species distributions under climate change (Urban et al., 2016). By incorporating these factors, our understanding of the disease risk hotspots can be refined further. Future studies aimed at understanding how disease risk changes with biodiversity may also benefit from incorporating differences in pathogen competence among species (Downs et al., 2019; Han et al., 2015). Other species traits, such as group size, home range size, trophic level, feeding style, or social behaviour, can also further improve models. We expect that these relationships differ among pathogens and that host phylogeny is important too (Albery et al., 2020; Huang et al., 2019; Wang et al., 2019). Despite these uncertainties, our predicted disease risk calculated from mammal assemblages explained about 30% of the variance in EIDs in humans. Of course, EIDs in humans can also be related to human activities and environments (Allen et al., 2017), which were not included in our analyses.

Our global disease risk estimation from mammal assemblage composition corresponds well with spatial patterns in EID outbreaks (Allen et al., 2017). Disease risk was not only predicted to be high in tropical areas, where biodiversity is highest (Allen et al., 2017; Hay et al., 2013), but also in temperate areas. Mammal assemblages with more small-bodied species or with increasing abundances of these species were associated with greater risks of disease outbreaks.

While many previous studies of disease–diversity relationships have focused on species losses (i.e. reductions in SR), we show that substantial changes in disease risk can occur without the local extinctions of any species. This shift in perspective has important implications for future studies of disease risk dynamics. Understanding changes in the absolute and relative abundance of competent and incompetent hosts is pivotal for predicting disease risk. In contrast, continued focus on local (or global) extinction may underestimate changes in disease risk and even stimulate inadequate public health and nature conservation policies.

ACKNOWLEDGEMENTS

We are grateful to A. Dobson for his valuable suggestions on the manuscript. This research is funded by the National Natural Science Foundation of China (no. 31870400) and Chinese Scholarship Council (no. 201506190134). The research of Z.Y.X.H is also supported by the Priority Academic Programme Development (PAPD) of Jiangsu Higher Education Institutions.

CONFLICT OF INTEREST

The authors declare no competing interests.

AUTHOR CONTRIBUTION

Willem F. de Boer, Yingying X.G. Wang, Kevin D. Matson, and Zheng Y.X. Huang designed the study. Luca Santini and Piero Visconti carried out the modelling of species distribution and abundance estimation. Toph Allen provided the additional data. Yingying X.G. Wang performed the disease risk modelling and statistical analysis. Yingying X.G. Wang, Kevin D. Matson, Zheng Y.X. Huang, and Willem F. de Boer wrote the first draft of paper; Luca Santini and Piero Visconti wrote the methods parts about species distribution and species abundance estimation. Yingying X.G. Wang, Luca Santini, Kevin D. Matson, Yingying X.G. Wang, and Willem F. de Boer revised the paper based on contributions of Jelle P. Hilbers, Mark A.J. Huijbregts, Yanjie Xu, Herbert H.T. Prins, and Toph Allen.

DATA AVAILABILITY STATEMENT

Species current range maps, together with the data of species' habitat preference and tolerance to human disturbance, were collected from IUCN Red List (https://www.iucnredlist.org/); Climatic and land-use data are available from ISIMIP node of the ESG server (https://esg.pik-potsdam.de/search/isimip/product=input); Body mass and diet data were collected from the EltonTrait databank (Wilman et al., 2014; http://www.esapubs.org/archive/ecol/E095/178/); Abundance data for fitting models were collected from the TetraDENSITY dataset (https://figshare.com/articles/dataset/TetraDENSITY_Population_Density_dataset/5371633).

ORCID

Yingying X. G. Wang https://orcid.org/0000-0003-3066-197X
Kevin D. Matson https://orcid.org/0000-0002-4373-5926
Luca Santini https://orcid.org/0000-0002-5418-3688
Piero Visconti https://orcid.org/0000-0001-6823-2826
Jelle P. Hilbers https://orcid.org/0000-0002-9401-589X
Mark A. J. Huijbregts https://orcid.org/0000-0002-7037-680X
Yanjie Xu https://orcid.org/0000-0003-4420-6353
Herbert H. T. Prins https://orcid.org/0000-0003-1131-5107
Toph Allen https://orcid.org/0000-0003-4580-091X
Zheng Y. X. Huang https://orcid.org/0000-0002-8761-3787
Willem F. de Boer https://orcid.org/0000-0003-3208-8521

REFERENCES

Albery, G. F., Eskew, E. A., Ross, N., & Olival, K. J. (2020). Predicting the global mammalian viral sharing network using phylogeography. *Nature Communications*, *11*(1), 1–9. https://doi.org/10.1038/s41467-020-16153-4

Allen, T., Murray, K. A., Zambrana-Torrelio, C., Morse, S. S., Rondinini, C., Di Marco, M., Breit, N., Olival, K. J., & Daszak, P. (2017). Global hotspots and correlates of emerging zoonotic diseases. *Nature Communications*, *8*(1), 1124. https://doi.org/10.1038/s41467-017-00923-8

Allouche, O., Tsoar, A., & Kadmon, R. (2006). Assessing the accuracy of species distribution models: Prevalence, kappa and the true skill statistic (TSS). *Journal of Applied Ecology*, *43*(6), 1223–1232. https://doi.org/10.1111/j.1365-2664.2006.01214.x

Altizer, S., Nunn, C. L., Thrall, P. H., Gittleman, J. L., Antonovics, J., Cunningham, A. A., Dobson, A. P., Ezenwa, V., Jones, K. E., Pedersen, A. B., Poss, M., & Pulliam, J. R. C. (2003). Social organization and parasite risk in mammals: Integrating theory and empirical studies. *Annual Review of Ecology, Evolution, and Systematics*, *34*(1), 517–547. https://doi.org/10.1146/annurev.ecolsys.34.030102.151725

Ameca y Juárez, E. I., Mace, G. M., Cowlishaw, G., Cornforth, W. A., & Pettorelli, N. (2013). Assessing exposure to extreme climatic events for terrestrial mammals. *Conservation Letters*, *6*(3), 145–153. https://doi.org/10.1111/j.1755-263X.2012.00306.x

Banerjee, S., Perelson, A. S., & Moses, M. (2017). Modelling the effects of phylogeny and body size on within-host pathogen replication and immune response. *Journal of the Royal Society Interface*, *14*(136), 20170479. https://doi.org/10.1098/rsif.2017.0479

Beaumont, L. J., Graham, E., Duursma, D. E., Wilson, P. D., Cabrelli, A., Baumgartner, J. B., Hallgren, W., Esperón-Rodríguez, M., Nipperess, D. A., Warren, D. L., Laffan, S. W., & VanDerWal, J. (2016). Which species distribution models are more (or less) likely to project broad-scale, climate-induced shifts in species ranges? *Ecological Modelling*, *342*, 135–146. https://doi.org/10.1016/j.ecolmodel.2016.10.004

Brooks, T. M., Pimm, S. L., Akçakaya, H. R., Buchanan, G. M., Butchart, S. H. M., Foden, W., Hilton-Taylor, C., Hoffmann, M., Jenkins, C. N., Joppa, L., Li, B. V., Menon, V., Ocampo-Peñuela, N., & Rondinini, C. (2019). Measuring terrestrial area of habitat (AOH) and its utility for the IUCN Red List. *Trends in Ecology & Evolution*, *34*(11), 977–986. https://doi.org/10.1016/j.tree.2019.06.009

Cardillo, M., Mace, G. M., Jones, K. E., Bielby, J., Bininda-Emonds, O. R., Sechrest, W., Orme, C. D. L., & Purvis, A. (2005). Multiple causes of high extinction risk in large mammal species. *Science*, *309*(5738), 1239–1241. https://doi.org/10.1126/science.1116030

Chen, L., & Zhou, S. (2015). A combination of species evenness and functional diversity is the best predictor of disease risk in multihost communities. *The American Naturalist*, *186*(6), 755–765. https://doi.org/10.1086/683774

Civitello, D. J., Cohen, J., Fatima, H., Halstead, N. T., Liriano, J., McMahon, T. A., Ortega, C. N., Sauer, E. L., Sehgal, T., Young, S., & Rohr, J. R. (2015). Biodiversity inhibits parasites: Broad evidence for the dilution effect. *Proceedings of the National Academy of Sciences of the United States of America*, *112*(28), 8667–8671. https://doi.org/10.1073/pnas.1506279112

Cleaveland, S., Laurenson, M., & Taylor, L. (2001). Diseases of humans and their domestic mammals: Pathogen characteristics, host range and the risk of emergence. *Philosophical Transactions of the Royal Society B: Biological Sciences*, *356*(1411), 991–999. https://doi.org/10.1098/rstb.2001.0889

Cronin, J. P., Rúa, M. A., & Mitchell, C. E. (2014). Why is living fast dangerous? Disentangling the roles of resistance and tolerance of disease. *The American Naturalist*, *184*(2), 172–187. https://doi.org/10.1086/676854

Damuth, J. (1981). Population density and body size in mammals. *Nature*, *290*(5808), 699–700. https://doi.org/10.1038/290699a0

Daszak, P., Cunningham, A. A., & Hyatt, A. D. (2000). Emerging infectious diseases of wildlife – Threats to biodiversity and human health. *Science*, *287*(5452), 443–449. https://doi.org/10.1126/science.287.5452.443

De Leo, G. A., & Dobson, A. P. (1996). Allometry and simple epidemic models for microparasites. *Nature*, *379*(6567), 720–722. https://doi.org/10.1038/379720a0

Díaz, S., Settele, J., Brondízio, E. S., Ngo, H. T., Agard, J., Arneth, A., Balvanera, P., Brauman, K. A., Butchart, S. H., & Chan, K. M. (2019). Pervasive human-driven decline of life on Earth points to the need for transformative change. *Science*, *366*(6471). https://doi.org/10.1126/science.aax3100

Dobson, A. (2004). Population dynamics of pathogens with multiple host species. *The American Naturalist*, *164*(5), S64–S78. https://doi.org/10.1086/424681

Downs, C. J., Dochtermann, N. A., Ball, R., Klasing, K. C., & Martin, L. B. (2020). The effects of body mass on immune cell concentrations of mammals. *The American Naturalist*, *195*(1), 107–114. https://doi.org/10.1086/706235

Downs, C. J., Schoenle, L. A., Han, B. A., Harrison, J. F., & Martin, L. B. (2019). Scaling of host competence. *Trends in Parasitology*, *35*(3), 182–192. https://doi.org/10.1016/j.pt.2018.12.002

Gaston, K. J., & Fuller, R. A. (2008). Commonness, population depletion and conservation biology. *Trends in Ecology & Evolution*, *23*(1), 14–19. https://doi.org/10.1016/j.tree.2007.11.001

Gibb, R., Redding, D. W., Chin, K. Q., Donnelly, C. A., Blackburn, T. M., Newbold, T., & Jones, K. E. (2020). Zoonotic host diversity increases in human-dominated ecosystems. *Nature*, *584*(7821), 398–402. https://doi.org/10.1038/s41586-020-2562-8

González-Suárez, M., Gómez, A., & Revilla, E. (2013). Which intrinsic traits predict vulnerability to extinction depends on the actual threatening processes. *Ecosphere*, *4*(6), 1–16. https://doi.org/10.1890/es12-00380.1

Halliday, F. W., & Rohr, J. R. (2019). Measuring the shape of the biodiversity-disease relationship across systems reveals new findings and key gaps. *Nature Communications*, *10*(1), 1–10. https://doi.org/10.1038/s41467-019-13049-w

Halliday, F. W., Rohr, J. R., & Laine, A. L. (2020). Biodiversity loss underlies the dilution effect of biodiversity. *Ecology Letters*, *23*(11), 1611–1622. https://doi.org/10.1111/ele.13590

Han, B. A., Kramer, A. M., & Drake, J. M. (2016). Global patterns of zoonotic disease in mammals. *Trends in Parasitology*, *32*(7), 565–577. https://doi.org/10.1016/j.pt.2016.04.007

Han, B. A., Park, A. W., Jolles, A. E., & Altizer, S. (2015). Infectious disease transmission and behavioural allometry in wild mammals. *Journal of Animal Ecology*, *84*(3), 637–646. https://doi.org/10.1111/1365-2656.12336

Hay, S. I., Battle, K. E., Pigott, D. M., Smith, D. L., Moyes, C. L., Bhatt, S., Brownstein, J. S., Collier, N., Myers, M. F., George, D. B., & Gething, P. W. (2013). Global mapping of infectious disease. *Philosophical Transactions of the Royal Society B: Biological Sciences*, *368*(1614), 20120250. https://doi.org/10.1098/rstb.2012.0250

Hillebrand, H., Bennett, D. M., & Cadotte, M. W. (2008). Consequences of dominance: A review of evenness effects on local and regional ecosystem processes. *Ecology*, *89*(6), 1510–1520. https://doi.org/10.1890/07-1053.1

Hof, C., Voskamp, A., Biber, M. F., Böhning-Gaese, K., Engelhardt, E. K., Niamir, A., Willis, S. G., & Hickler, T. (2018). Bioenergy cropland expansion may offset positive effects of climate change mitigation for global vertebrate diversity. *Proceedings of the National Academy of Sciences of the United States of America*, *115*(52), 13294–13299. https://doi.org/10.1073/pnas.1807745115

Huang, Z. Y. X., de Boer, W. F., van Langevelde, F., Olson, V., Blackburn, T. M., & Prins, H. H. T. (2013). Species' life-history traits explain interspecific variation in reservoir competence: A possible mechanism underlying the dilution effect. *PLoS One*, *8*(1), e54341. https://doi.org/10.1371/journal.pone.0054341

Huang, Z. Y. X., Van langevelde, F., Estrada-peña, A., Suzán, G., & De boer, W. F. (2016). The diversity–disease relationship: Evidence for and criticisms of the dilution effect. *Parasitology*, *143*, 1075–1086. https://doi.org/10.1017/S0031182016000536

Huang, Z. Y. X., Xu, C., van Langevelde, F., Ma, Y., Langendoen, T., Mundkur, T., Si, Y., Tian, H., Kraus, R. H., Gilbert, M., Han, G.-Z., Ji, X., Prins, H. H. T., & De Boer, W. F. (2019). Contrasting effects of host species and phylogenetic diversity on the occurrence of HPAI H5N1 in European wild birds. *Journal of Animal Ecology*, *88*(7), 1044–1053. https://doi.org/10.1111/1365-2656.12997

Huang, Z. Y. X., Yu, Y., van Langevelde, F., & de Boer, W. F. (2017). Does the dilution effect generally occur in animal diseases? *Parasitology*, *144*(6), 823–826. https://doi.org/10.1017/S0031182016002572

IUCN. (2015). *The IUCN Red List of Threatened Species*, *version 2015-4*. IUCN.

Johnson, P. T., Calhoun, D. M., Riepe, T., McDevitt-Galles, T., & Koprivnikar, J. (2019). Community disassembly and disease: Realistic—but not randomized—biodiversity losses enhance parasite transmission. *Proceedings of the Royal Society B: Biological Sciences*, *286*(1902), 20190260. https://doi.org/10.1098/rspb.2019.0260

Johnson, P. T., Rohr, J. R., Hoverman, J. T., Kellermanns, E., Bowerman, J., & Lunde, K. B. (2012). Living fast and dying of infection: Host life history drives interspecific variation in infection and disease risk. *Ecology Letters*, *15*(3), 235–242. https://doi.org/10.1111/j.1461-0248.2011.01730.x

Jones, K. E., Patel, N. G., Levy, M. A., Storeygard, A., Balk, D., Gittleman, J. L., & Daszak, P. (2008). Global trends in emerging infectious diseases. *Nature*, *451*(7181), 990–993. https://doi.org/10.1038/nature06536

Joseph, M. B., Mihaljevic, J. R., Orlofske, S. A., & Paull, S. H. (2013). Does life history mediate changing disease risk when communities disassemble? *Ecology Letters*, *16*(11), 1405–1412. https://doi.org/10.1111/ele.12180

Jung, M., Dahal, P. R., Butchart, S. H., Donald, P. F., De Lamo, X., Lesiv, M., Kapos, V., Rondinini, C., & Visconti, P. (2020). A global map of terrestrial habitat types. *Scientific Data*, *7*(1), 1–8. https://doi.org/10.1038/s41597-020-00599-8

Keesing, F., & Ostfeld, R. S. (2021). Impacts of biodiversity and biodiversity loss on zoonotic diseases. *Proceedings of the National Academy of Sciences of the United States of America*, *118*(17), e2023540118. https://doi.org/10.1073/pnas.2023540118

Liu, X., Chen, L., Liu, M., García-Guzmán, G., Gilbert, G. S., & Zhou, S. (2020). Dilution effect of plant diversity on infectious diseases: Latitudinal trend and biological context dependence. *Oikos*, *129*(4), 457–465. https://doi.org/10.1111/oik.07027

McGill, B. J., Dornelas, M., Gotelli, N. J., & Magurran, A. E. (2015). Fifteen forms of biodiversity trend in the Anthropocene. *Trends in Ecology & Evolution*, *30*(2), 104–113. https://doi.org/10.1016/j.tree.2014.11.006

Merrill, T. E. S., & Johnson, P. T. (2020). Towards a mechanistic understanding of competence: A missing link in diversity–disease research. *Parasitology*, *147*(11), 1159–1170. https://doi.org/10.1017/s0031182020000943

Newbold, T. (2018). Future effects of climate and land-use change on terrestrial vertebrate community diversity under different scenarios.

Proceedings of the Royal Society B: Biological Sciences, *285*(1881), 20180792. https://doi.org/10.1098/rspb.2018.0792

O'Neill, B. C., Kriegler, E., Riahi, K., Ebi, K. L., Hallegatte, S., Carter, T. R., Mathur, R., & van Vuuren, D. P. (2014). A new scenario framework for climate change research: The concept of shared socioeconomic pathways. *Climatic Change*, *122*(3), 387–400. https://doi.org/10.1007/s10584-013-0905-2

Ostfeld, R. S., & Keesing, F. (2012). Effects of host diversity on infectious disease. *Annual Review of Ecology Evolution and Systematics*, *43*, 157–182. https://doi.org/10.1146/annurev-ecolsys-102710-145022

Ostfeld, R. S., Levi, T., Jolles, A. E., Martin, L. B., Hosseini, P. R., & Keesing, F. (2014). Life history and demographic drivers of reservoir competence for three tick-borne zoonotic pathogens. *PLoS One*, *9*(9), e107387. https://doi.org/10.1371/journal.pone.0107387

Peters, R. H. (1986). *The ecological implications of body size* (Vol. *2*). Cambridge University Press.

Randolph, S. E., & Dobson, A. D. M. (2012). Pangloss revisited: A critique of the dilution effect and the biodiversity-buffers-disease paradigm. *Parasitology*, *139*(7), 847–863. https://doi.org/10.1017/S0031182012000200

Ricklefs, R. E., & Wikelski, M. (2002). The physiology/life-history nexus. *Trends in Ecology & Evolution*, *17*(10), 462–468. https://doi.org/10.1016/S0169-5347(02)02578-8

Roberts, D. R., Bahn, V., Ciuti, S., Boyce, M. S., Elith, J., Guillera-Arroita, G., Hauenstein, S., Lahoz-Monfort, J. J., Schröder, B., Thuiller, W., Warton, D. I., Wintle, B. A., Hartig, F., & Dormann, C. F. (2017). Cross-validation strategies for data with temporal, spatial, hierarchical, or phylogenetic structure. *Ecography*, *40*(8), 913–929. https://doi.org/10.1111/ecog.02881

Rohr, J. R., Civitello, D. J., Halliday, F. W., Hudson, P. J., Lafferty, K. D., Wood, C. L., & Mordecai, E. A. (2020). Towards common ground in the biodiversity–disease debate. *Nature Ecology & Evolution*, *4*(1), 24–33. https://doi.org/10.1038/s41559-019-1060-6

Rondinini, C., Di Marco, M., Chiozza, F., Santulli, G., Baisero, D., Visconti, P., Hoffmann, M., Schipper, J., Stuart, S. N., Tognelli, M. F., Amori, G., Falcucci, A., Maiorano, L., & Boitani, L. (2011). Global habitat suitability models of terrestrial mammals. *Philosophical Transactions of the Royal Society B: Biological Sciences*, *366*(1578), 2633–2641. https://doi.org/10.1098/rstb.2011.0113

Rowlands, D. J., Frame, D. J., Ackerley, D., Aina, T., Booth, B. B. B., Christensen, C., Collins, M., Faull, N., Forest, C. E., Grandey, B. S., Gryspeerdt, E., Highwood, E. J., Ingram, W. J., Knight, S., Lopez, A., Massey, N., McNamara, F., Meinshausen, N., Piani, C., … Allen, M. R. (2012). Broad range of 2050 warming from an observationally constrained large climate model ensemble. *Nature Geoscience*, *5*(4), 256–260. https://doi.org/10.1038/ngeo1430

Rudolf, V. H., & Antonovics, J. (2005). Species coexistence and pathogens with frequency-dependent transmission. *The American Naturalist*, *166*(1), 112–118. https://doi.org/10.1086/430674

Salkeld, D. J., Padgett, K. A., & Jones, J. H. (2013). A meta-analysis suggesting that the relationship between biodiversity and risk of zoonotic pathogen transmission is idiosyncratic. *Ecology Letters*, *16*(5), 679–686. https://doi.org/10.1111/Ele.12101

Santini, L., Butchart, S. H., Rondinini, C., Benítez-López, A., Hilbers, J. P., Schipper, A. M., Cengic, M., Tobias, J. A., & Huijbregts, M. A. (2019). Applying habitat and population-density models to land-cover time series to inform IUCN Red List assessments. *Conservation Biology*, *33*(5), 1084–1093. https://doi.org/10.1111/cobi.13279

Santini, L., Isaac, N. J., & Ficetola, G. F. (2018). TetraDENSITY: A database of population density estimates in terrestrial vertebrates. *Global Ecology and Biogeography*, *27*(7), 787–791. https://doi.org/10.1111/geb.12756

Santini, L., Isaac, N. J., Maiorano, L., Ficetola, G. F., Huijbregts, M. A., Carbone, C., & Thuiller, W. (2018). Global drivers of population density in terrestrial vertebrates. *Global Ecology and Biogeography*, *27*(8), 968–979. https://doi.org/10.1111/geb.12758

Silva, M., Brown, J. H., & Downing, J. A. (1997). Differences in population density and energy use between birds and mammals: A macroecological perspective. *The Journal of Animal Ecology*, *66*(3), 327–340. https://doi.org/10.2307/5979

Silva, M., & Downing, J. A. (1995). The allometric scaling of density and body mass: A nonlinear relationship for terrestrial mammals. *The American Naturalist*, *145*(5), 704–727. https://doi.org/10.1086/285764

Thuiller, W., Guéguen, M., Renaud, J., Karger, D. N., & Zimmermann, N. E. (2019). Uncertainty in ensembles of global biodiversity scenarios. *Nature Communications*, *10*(1), 1–9. https://doi.org/10.1038/s41467-019-09519-w

Tomiya, S. (2013). Body size and extinction risk in terrestrial mammals above the species level. *The American Naturalist*, *182*(6), E196–E214. https://doi.org/10.1086/673489

Urban, M. C., Bocedi, G., Hendry, A. P., Mihoub, J.-B., Peer, G., Singer, A., Bridle, J. R., Crozier, L. G., De Meester, L., Godsoe, W., Gonzalez, A., Hellmann, J. J., Holt, R. D., Huth, A., Johst, K., Krug, C. B., Leadley, P. W., Palmer, S. C. F., Pantel, J. H., … Travis, J. M. J. (2016). Improving the forecast for biodiversity under climate change. *Science*, *353*(6304). https://doi.org/10.1126/science.aad8466

Visconti, P., Bakkenes, M., Baisero, D., Brooks, T., Butchart, S. H. M., Joppa, L., Alkemade, R., Di Marco, M., Santini, L., Hoffmann, M., Maiorano, L., Pressey, R. L., Arponen, A., Boitani, L., Reside, A. E., van Vuuren, D. P., & Rondinini, C. (2016). Projecting global biodiversity indicators under future development scenarios. *Conservation Letters*, *9*(1), 5–13. https://doi.org/10.1111/conl.12159

Visconti, P., Pressey, R. L., Giorgini, D., Maiorano, L., Bakkenes, M., Boitani, L., Alkemade, R., Falcucci, A., Chiozza, F., & Rondinini, C. (2011). Future hotspots of terrestrial mammal loss. *Philosophical Transactions of the Royal Society B: Biological Sciences*, *366*(1578), 2693–2702. https://doi.org/10.1098/rstb.2011.0105

Wang, Y. X. G., Matson, K. D., Prins, H. H. T., Gort, G., Awada, L., Huang, Z. Y. X., & de Boer, W. F. (2019). Phylogenetic structure of wildlife assemblages shapes patterns of infectious livestock diseases in Africa. *Functional Ecology*, *33*(7), 1332–1343. https://doi.org/10.1111/1365-2435.13311

Wilman, H., Belmaker, J., Simpson, J., de la Rosa, C., Rivadeneira, M. M., & Jetz, W. (2014). EltonTraits 1.0: Species-level foraging attributes of the world's birds and mammals: Ecological Archives E095–178. *Ecology*, *95*(7), 2027. https://doi.org/10.1890/13-1917.1

Wood, C. L., & Lafferty, K. D. (2013). Biodiversity and disease: A synthesis of ecological perspectives on Lyme disease transmission. *Trends in Ecology & Evolution*, *28*(4), 239–247. https://doi.org/10.1016/j.tree.2012.10.011

Wood, C. L., Lafferty, K. D., DeLeo, G., Young, H. S., Hudson, P. J., & Kuris, A. M. (2014). Does biodiversity protect humans against infectious disease? *Ecology*, *95*(4), 817–832. https://doi.org/10.1890/13-1041.1

SUPPORTING INFORMATION

Additional supporting information may be found online in the Supporting Information section.

How to cite this article: Wang, Y. X. G., Matson, K. D., Santini, L., Visconti, P., Hilbers, J. P., Huijbregts, M. A. J., Xu, Y., Prins, H. H. T., Allen, T., Huang, Z. Y. X., & de Boer, W. F. (2021). Mammal assemblage composition predicts global patterns in emerging infectious disease risk. *Global Change Biology*, 27, 4995–5007. https://doi.org/10.1111/gcb.15784